ISSN: 2754-4753

Journal of Physics & Optics Sciences

Research Article

Open Access

New Analytical Models in Conformal Symmetry with Strange Equation of State

Manuel Malaver

Department of Basic Sciences, Maritime University of the Caribbean, Catia la Mar, Venezuela

Institute of Scholars, Muddhinapalya Bengaluru-560091, Karnataka, India

Department of Applied Physics, Engineering Faculty, Central University of Venezuela, Venezuela

ABSTRACT

In this study, we obtained new classes of solutions to the Einstein-Maxwell field equations for charged anisotropic compact stars with a matter equation of state provided by the MIT bag model when conformal symmetry is present. With an electromagnetic field, the new solutions can be expressed in terms of elementary and polynomial functions. The produced solutions meet every physical requirement for models of realistic compact stars. The mass function and surface redshift are comparable with the reported experimental data of stellar binary system 4U1702-429.

***Corresponding author**

Manuel Malaver, Department of Basic Sciences, Maritime University of the Caribbean, Catia la Mar, Venezuela.

Received: October 22, 2025; **Accepted:** November 02, 2025; **Published:** November 10, 2025

Keywords: Conformal Symmetry, MIT Bag Model, Compact Stars, Polynomial Functions, Electromagnetic Field

Introduction

Most galaxies have clouds of gas and dust with a non-uniform distribution of mass, which is where stars are formed. White dwarfs and neutron stars that originate close to the conclusion of their stellar evolution are typically referred to as "compact objects" in astronomy [1-2]. Compact objects are characterized by high densities and strong gravitational fields. Albert Einstein created the General Theory of Relativity (GR) in 1915 to study strong gravitational forces. The idea is thought to be the basic foundation for stellar astrophysics research. The Einstein Field Equations (EFEs) can be used to study and comprehend the structure and behavior of astronomical objects. In 1916, Schwarzschild developed the first solution to the EFEs [3]. Since then, several researchers have looked at these equations in different ways, and several astrophysical models have been created to provide a comprehensive explanation of how mass is distributed within star bodies [4-6]. The GR theory characterizes gravity as a geometric property of space and time by generalizing special relativity and extending Newton's law of universal gravitation [7-8]. The EFEs for compact star models have currently been solved by a number of researches [9-17].

Anisotropy pressure in star objects in the presence of high gravitational fields is a topic of vital importance for many astrophysics experts. Phase transitions are factors of neutron star evolution that can cause anisotropy, according to Sokolov [18]. Anisotropy can also result from the presence of an electrical field [19]. Anisotropy can alter the structure of compact objects, according to Bowers and Liang [20]. Because radial forces of different signs arise in the star interior, disrupting the system balance, Herrera et al. [21] concludes that pressure anisotropy affects matter stability. According to Thirukkanesh and Ragel [22], anisotropy has an impact on the structure and certain physical properties of compact stars, such as mass and compactness. Additionally, some research has created anisotropic models (Mak and Harko [23], Takisa and Maharaj [26], Malaver [27-28], Thirukkanesh and Ragel [25], Malaver and Iyer [24], and Thirukkanesh and Ragel [22]).

Studying the characteristics and behavior of compact stars has also benefited from the application of conformal symmetry. These potentials are subject to certain restrictions that make the solution of the field equations easier when the conformal Killing vector is applied to the space-time manifold. In the past, some authors have studied conformal symmetry and equations of state with single-layered stars [29-30]. A relativistic compact star model with a linear equation of state and a conformal Killing vector in the presence of charge was created by Jape et al. [31]. In addition to the conformal Killing vector, Christopher et al. [32] used a quadratic equation of state to study the properties of a relativistic charged compact star. In the core-envelope situation, Kowa et al. [33] derived new solutions to the Einstein field equations by combining the conformal Killing vector with multiple equations of state for double-layered stars. An electrically charged anisotropic fluid sphere connected to the Reissner-Nordstrom static solution via a zero-pressure surface yielded new families of compact solutions for a spherically symmetric distribution of matter, according to

Esculpi and Aloma [34]. Malaver and Esculpi [35] proposed some new stellar configurations that represent models of dark energy stars in presence of a conformal Killing vector with the linear equation of state.

In this work, we combine a linear equation of state and the Conformal Killing Vector (CKV) to examine the physics and behavior of a charged anisotropic star. In Sec. 2, the Einstein-Maxwell field equations used to generate the model are presented. We give a detailed description of conformal Killing Vector in Sec. 3. By choosing of a gravitational potential that allow the field equations to be solved, we construct new models for charged anisotropic matter in section 4. In Section 5, the physical acceptability requirements are discussed. The validity and physical properties of these new solutions are examined in Section 6. The concluding remarks are provided in Section 7

Field Equations

We examine a static, homogeneous, anisotropic, spherically symmetric spacetime in Schwarzschild coordinates, which is provided by

$$ds^2 = -e^{2\nu(r)}dt^2 + e^{2\lambda(r)}dr^2 + r^2(d\theta^2 + \sin^2\theta d\varphi^2) \quad (1)$$

where $\nu(r)$ and $\lambda(r)$ are two arbitrary functions.

Given the charged anisotropic matter, the Einstein field equations are

$$\frac{1}{r^2}\left(1-e^{-2\lambda}\right)+\frac{2\lambda'}{r}e^{-2\lambda} = \rho + \frac{1}{2}E^2 \quad (2)$$

$$-\frac{1}{r^2}\left(1-e^{-2\lambda}\right)+\frac{2\nu'}{r}e^{-2\lambda} = p_r - \frac{1}{2}E^2 \quad (3)$$

$$e^{-2\lambda}\left(\nu''+\nu'^2+\frac{\nu'}{r}-\nu'\lambda'-\frac{\lambda'}{r}\right) = p_t + \frac{1}{2}E^2 \quad (4)$$

$$\sigma = \frac{1}{r^2}e^{-\lambda}(r^2E)' \quad (5)$$

where ρ is the energy density, p_r is the radial pressure, E is electric field intensity and p_t is the tangential pressure, respectively.
Using the transformations of Durgapal and Using the transformations of Durgapal and Bannerji [36], $x = cr^2$, $Z(x) = e^{-2\lambda(r)}$ and $A_c^2 y^2(x) = e^{2\nu(r)}$ with arbitrary constants A_c and c>0 the metric (1) take the form

$$ds^2 = -A^2y^2(x)dt^2 + \frac{dx^2}{4Z(x)Cx} + \frac{x}{C}(d\theta^2 + \sin^2\theta d\varphi^2)$$

and the Einstein field equations can be written as

$$\frac{1-Z}{x} - 2\dot{Z} = \frac{\rho}{c} + \frac{E^2}{2c} \quad (6)$$

$$4Z\frac{\dot{y}}{y} - \frac{1-Z}{x} = \frac{p_r}{c} - \frac{E^2}{2c} \quad (7)$$

$$4xZ\frac{\ddot{y}}{y} + (4Z+2x\dot{Z})\frac{\dot{y}}{y} + \dot{Z} = \frac{p_t}{c} + \frac{E^2}{2c} \quad (8)$$

$$p_t = p_r + \Delta \quad (9)$$

$$\frac{\Delta}{c} = 4xZ\frac{\ddot{y}}{y} + \dot{Z}\left(1+2x\frac{\dot{y}}{y}\right) + \frac{1-Z}{x} - \frac{E^2}{c} \quad (10)$$

$$\sigma^2 = \frac{4cZ}{x}\left(x\dot{E}+E\right)^2 \quad (11)$$

σ is the charge density and dots denoting differentiation with respect to x. With the transformations in [36], the mass within a radius r of the sphere take the form

$$M(x) = \frac{1}{4c^{3/2}}\int_0^x \sqrt{x}\,\rho(x)dx \quad (12)$$

The interior metric (1) with the charged matter distribution should match the exterior spacetime described by the Reissner-Nordström metric:

$$ds^2 = -\left(1-\frac{2M}{r}+\frac{Q^2}{r^2}\right)dt^2 + \left(1-\frac{2M}{r}+\frac{Q^2}{r^2}\right)^{-1}dr^2 + r^2(d\theta^2 + \sin^2\theta d\varphi^2) \quad (13)$$

where the total mass and the total charge of the star are denoted by M and q^2, respectively. The junction conditions at the stellar surface are obtained by matching the first and the second fundamental forms for the interior metric (1) and the exterior metric (13).

In this paper, we assume the following linear equation of state defined as

$$p_r = \alpha\rho - \beta \quad (14)$$

where α and β are real constants such that $\alpha \neq 0$.

Conformal Symmetry

We examine the manifold of spacetime that admits conformal symmetry. The system's EFEs (2-4) are made simpler by the Conformal Killing Vector's imposition (CKV). The application of CKV results in new exact solutions for the core-envelope model in conjunction with the equation of state. The conformal Killing vector is defined as [37]

$$LX(r,t)g_{ab} = 2\phi(r,t)g_{ab} \quad (15)$$

where L is the Lie derivate operator, $X(r,t)$ stands for vector field, g_{ij} is the metric tensor $\phi(r,t)$ and is a conformal factor. With symmetry assumption, the conformal Killing vector and the conformal factor in (15) are given by

$$X = \alpha(t,r)\frac{\partial}{\partial t} + \beta(t,r)\frac{\partial}{\partial r} \quad (16)$$

$$\phi = \phi(r,t) \quad (17)$$

We take into account the related Weyl tensor integrability requirement [38] in order to solve equation (15)

$$LX(r,t)C^{i}_{jkl} = 0 \quad (18)$$

where C^{i}_{jkl} are the Weyl tensor components. With the eq. (18), eq. (15) can be expressed as

$$\nu'' + (\nu')^2 - \nu'\lambda' - \frac{\nu' - \lambda'}{r} + \frac{1}{r^2} = \frac{e^{2\lambda}(1+k)}{r^2} \quad (19)$$

where k represents a real constant.

With the transformations, $x = cr^2$, $Z(x) = e^{-2\lambda(r)}$ and $A_*^2 y^2(x) = e^{2\nu(r)}$ suggested for Durgapal & Bannerji [36] and the condition $k = 2(n-1)$ we obtain

$$y(x) = \begin{cases} A\sqrt{x}\exp\left(\frac{1}{2}\sqrt{2n-1}\int\frac{dx}{x\sqrt{Z}}\right) + B\sqrt{x}\exp\left(-\frac{1}{2}\sqrt{2n-1}\int\frac{dx}{x\sqrt{Z}}\right) \to n > 1/2 \\ A\frac{\sqrt{x}}{2}\int\frac{dx}{x\sqrt{Z}} + B\sqrt{x} \to n = 1/2 \\ A\sqrt{x}\exp\left(\frac{1}{2}\sqrt{-(2n-1)}\int\frac{dx}{x\sqrt{Z}}\right) + B\sqrt{x}\exp\left(-\frac{1}{2}\sqrt{-(2n-1)}\int\frac{dx}{x\sqrt{Z}}\right) \to n < 1/2 \end{cases} \quad (20)$$

where A and B are constant parameters and n=1 represents a conformally flat spacetime.

New Models

In this section, we found the novel solution for charged anisotropic compact stars that admits a linear equation of state and conformal symmetry. Substituting eq. (14) in the equations (6-7) for the electric field intensity we can obtain

$$\frac{E^2}{2C} = \left(\frac{1-Z}{x}\right) - 2\dot{Z} - \frac{1}{\alpha+1}\left(4Z\frac{\dot{y}}{y} - 2\dot{Z} + \frac{\beta}{C}\right) \quad (21)$$

where Z is the chosen metric potential that can be written as

$$Z(x) = \left(\frac{1-ax}{1+ax}\right)^2 \quad (22)$$

For the energy density and the radial pressure we have, respectively

$$\rho = \frac{C}{\alpha+1}\left(4Z\frac{\dot{y}}{y} - 2\dot{Z} + \frac{\beta}{C}\right) \quad (23)$$

$$P_r = \frac{\alpha C}{\alpha+1}\left(4Z\frac{\dot{y}}{y} - 2\dot{Z} + \frac{\beta}{C}\right) - \beta \quad (24)$$

With the conformal condition (20) and eq. (22) and considering case n=1, the second gravitational potential is written as

$$y(x) = \frac{Ax}{ax-1} + B(ax-1) \quad (25)$$

With the equations (21) and (22) and substituting eq. (23) in (6), we obtain for the energy density

$$\rho = \frac{C}{\alpha+1}\left(-\frac{4(1-ax)}{(1+ax)^2}\frac{\left[-A + aB(ax-1)^2\right]}{\left[Ax + B(ax-1)^2\right]} + \frac{8a(1-ax)}{(1+ax)^3} + \frac{\beta}{C}\right) \quad (26)$$

and for the radial pressure

$$P_r = \frac{\alpha C}{\alpha+1}\left(-\frac{4(1-ax)}{(1+ax)^2}\frac{\left[-A + aB(ax-1)^2\right]}{\left[Ax + B(ax-1)^2\right]} + \frac{8a(1-ax)}{(1+ax)^3} + \frac{\beta}{C}\right) - \beta \quad (27)$$

With the equations (22) and (25) and their derivatives, the electric field intensity can be written as

$$\frac{E^2}{2C} = \frac{4a(3-ax)}{(1+ax)^3} - \frac{1}{\alpha+1}\left(-4\frac{(1-ax)}{(1+ax)^2}\frac{\left[-A + aB(ax-1)^2\right]}{\left[Ax + B(ax-1)^2\right]} + \frac{8a(1-ax)}{(1+ax)^3} + \frac{\beta}{C}\right) \quad (28)$$

By comparison of line elements (1) and (13) and considering $E|_{r=R} = Q/R^2$ we obtained for the mass of the star

$$M(x) = \frac{1}{2}\sqrt{\frac{x}{C}}\left[1 - \frac{(1-ax)^2}{(1+ax)^2} + \frac{8ax(3-x)}{(1+ax)^3} - \frac{2x}{\alpha+1}\left\{\frac{4(1-ax)^2\left[-\frac{A}{(ax-1)^2} + aB\right]}{(1+ax)^2\left[\frac{Ax}{ax-1} + B(ax-1)\right]} + \frac{8a(1-ax)}{(1+ax)^3} + \frac{\beta}{C}\right\}\right] \quad (29)$$

With the equations (22) and (25), we have for the metric potentials

$$e^{2\lambda(r)} = \left(\frac{1+ax}{1-ax}\right)^2 \quad (30)$$

$$e^{2\nu(r)} = A_*^2\left(\frac{Ax}{ax-1} + B(ax-1)\right)^2 \quad (31)$$

and the measure of anisotropy Δ can be written as

$$\Delta = \frac{8aAx(1-ax)^2}{(1+ax)^2\left[Ax(ax-1)^2 + B(ax-1)^4\right]} - \frac{4a(1-ax)}{(1+ax)^3}\left\{1 + 2x\frac{\left[-A + aB(ax-1)^2\right]}{\left[Ax(ax-1) + B(ax-1)^3\right]}\right\} + \frac{4a}{(1+ax)^2} - \frac{8a(1-ax)}{(1+ax)^3} + \frac{2}{\alpha+1}\left[\frac{-4A(ax-1) + 4aB(ax-1)^3}{Ax(ax-1)^2 + B(a^2x^2-1)^2} + \frac{8a(1-ax)}{(1+ax)^3} + \frac{\beta}{C}\right] \quad (32)$$

Conditions for Physical Acceptability

For a model to be physically acceptable, the following conditions should be satisfied [39]:

(i) The metric potentials $e^{2\lambda}$ and $e^{2\nu}$ assume finite values throughout the stellar interior and are singularity-free at the center r=0.

(ii) The energy density ρ and radial pressure P_r should be positive and a decreasing function inside the star.

(iii) The radial pressure P_r should be zero at the boundary $r=R$.

(iv) The gradients in radial pressure and density $d\rho/dr \leq 0$ and $dP_r/dr \leq 0$ for $0 \leq r \leq R$.

(v) The anisotropy is zero at the center r=0, i.e. $\Delta(r=0) = 0$.

(vi) Any physically acceptable model must satisfy the causality condition, that is, for the radial sound speed $v_{sr}^2 = \frac{dP_r}{d\rho}$ must be satisfied that $0 \leq v_{sr}^2 \leq 1$

(vii) The charged interior solution should be matched with the Reissner-Nordström exterior solution, for which the metric is given by eq. (13).

The conditions (ii) and (iv) imply that the energy density must reach a maximum at the center and decrease towards the surface of the sphere.

The Physical Characteristics of the New Models

We now present the analysis of the physical characteristics for the new models. The metric functions $e^{2\lambda}$ and $e^{2\nu}$ have finite values and remain positive throughout the stellar interior. At the center $e^{2\lambda(0)}=1$ and $e^{2\nu(0)}=A_*^2B^2$. We show that in $r=0$ $\left(e^{2\lambda(r)}\right)'_{r=0}=\left(e^{2\nu(r)}\right)'_{r=0}=0$ and this make is possible to verify that the gravitational potentials are regular at the center. The energy density and radial pressure are positive and well behaved within the star. Also, we have for the central density and radial pressure $\rho(0)=\frac{4C}{\alpha+1}\left(\frac{A+aB}{B}+\frac{\beta}{4C}\right)$ and $P_r(0)=\frac{4\alpha C}{\alpha+1}\left(\frac{A+aB}{B}+\frac{\beta}{4C}\right)-\beta$

$$ds^2=-\left(1-\frac{2M}{r}+\frac{Q^2}{r^2}\right)dt^2+\left(1-\frac{2M}{r}+\frac{Q^2}{r^2}\right)^{-1}dr^2+r^2(d\theta^2+\sin^2\theta d\varphi^2)$$

and the continuity of e^{ν} and e^{λ} across the boundary $r=R$ is

$$e^{2\nu}=e^{-2\lambda}=1-\frac{2M}{R}+\frac{Q^2}{R^2} \quad (33)$$

Then, for the matching conditions, we obtain

$$\frac{2M}{R}=1-\left(\frac{1-aCR^2}{1+aCR^2}\right)^2+\frac{8aR^2\left(3-aCR^2\right)}{\left(1+aCR^2\right)^3} -\frac{2R^2}{\alpha+1}\left\{\frac{4\left(1-aCR^2\right)^2\left[-\frac{A}{\left(aCR^2-1\right)^2}+aB\right]}{\left(1+aCR^2\right)^2\left[\frac{ACR^2}{aCR^2-1}+B\left(aCR^2-1\right)\right]}+\frac{8a\left(1-aCR^2\right)}{\left(1+aCR^2\right)^3}+\frac{\beta}{C}\right\} \quad (34)$$

The electric field must disappear at the star's core for the solution to have any physical significance, i.e.

$$\frac{E^2}{2C}=12a-\frac{1}{\alpha+1}\left(\frac{4A-4aB}{B}+8a+\frac{\beta}{C}\right)=0 \quad (35)$$

Considering that α=1/3 and β=0.000075, the values of B will depend on the A parameter as follows

$$B=\frac{4A}{12a-\frac{\beta}{C}} \quad (36)$$

The metric for this model is

$$ds^2=-A_*^2\left(\frac{Ax}{ax-1}+B(ax-1)\right)^2dt^2+\frac{(1+ax)^2dx^2}{4(1-ax)^2Cx}+\frac{x}{C}(d\theta^2+\sin^2\theta d\varphi^2) \quad (37)$$

In the following table shows the values of B obtained for different values of A. For all cases a= 0.001, α= 1/3 and β=0.000075.

Table 1: Values of B obtained for different values of A with a = 0.001 and α = 1/3

A	a	β	B
0.0003	0.001	0.000075	0.100628930
0.0004	0.001	0.000075	0.134171907
0.0005	0.001	0.000075	0.167714884
0.0006	0.001	0.000075	0.201257861

The figures 1-10 represent the plots of $\frac{E^2}{2C}$, ρ, P_r, $e^{2\nu(r)}$, $e^{2\lambda(r)}$, M, Z_S, Δ, $\frac{d\rho}{dr}$ and $\frac{dP_r}{dr}$ with the radial coordinate for different values of A. In all the graphs we considered C=1.

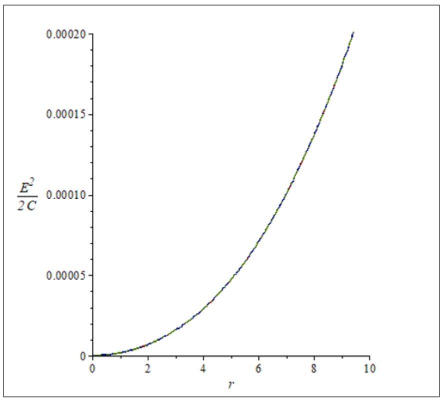

Figure 1: Electric field against the radial coordinate for A= 0.00003 (solid line), A= 0.00004 (long-dash line), A= 0.00005 (dash-dot line) and A=0.00006 (space-dot line). For all the cases a=0.001, α= 1/3 and β=0.000075.

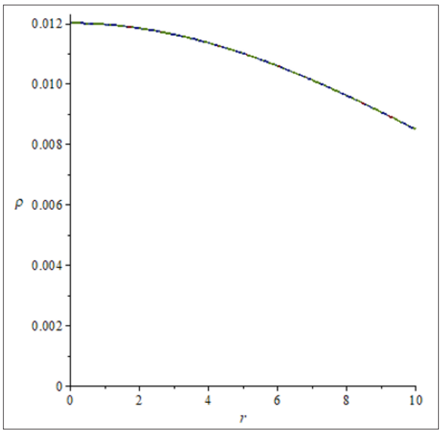

Figure 2: Energy density against the radial coordinate for A= 0.00003 (solid line), A= 0.00004 (long-dash line), A= 0.00005 (dash-dot line) and A=0.00006 (space-dot line). For all the cases a=0.001, α= 1/3 and β=0.000075

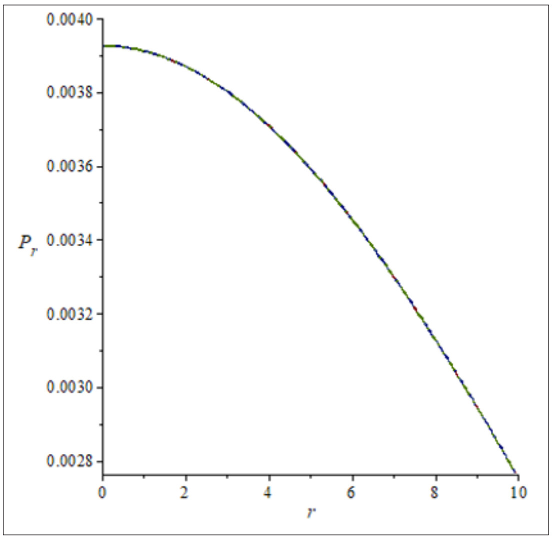

Figure 3: Radial pressure against the radial coordinate for A= 0.00003 (solid line), A= 0.00004 (long-dash line), A= 0.00005 (dash-dot line) and A=0.00006 (space-dot line). For all the cases a=0.001, α= 1/3 and β=0.000075

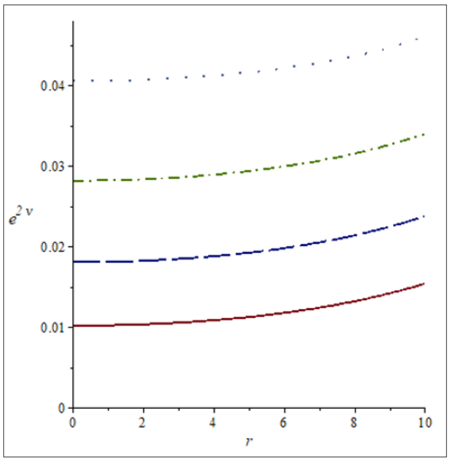

Figure 4: Metric potential $e^{2\nu}$ against the radial coordinate for A= 0.00003 (solid line), A= 0.00004 (long-dash line), A= 0.00005 (dash-dot line) and A=0.00006 (space-dot line). For all the cases a=0.001, α= 1/3 and β=0.000075

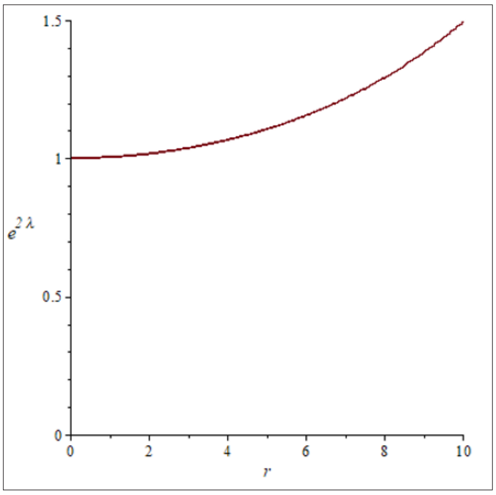

Figure 5: Metric potential $e^{2\lambda}$ against the radial coordinate for a=0.001

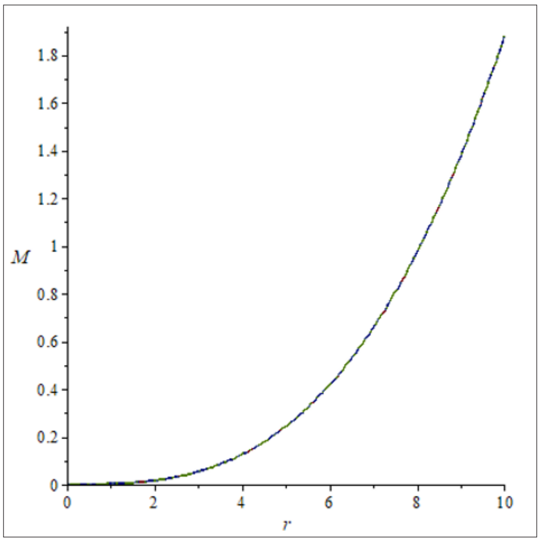

Figure 6: Mass against the radial coordinate for A= 0.00003 (solid line), A= 0.00004 (long-dash line), A= 0.00005 (dash-dot line) and A=0.00006 (space-dot line). For all the cases a=0.001, α= 1/3 and β=0.000075

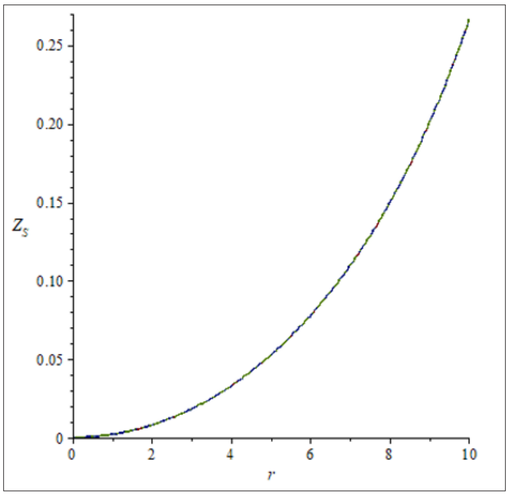

Figure 7: Surface redshift against the radial coordinate for A= 0.00003 (solid line), A= 0.00004 (long-dash line), A= 0.00005 (dash-dot line) and A=0.00006 (space-dot line). For all the cases a=0.001, α= 1/3 and β=0.000075

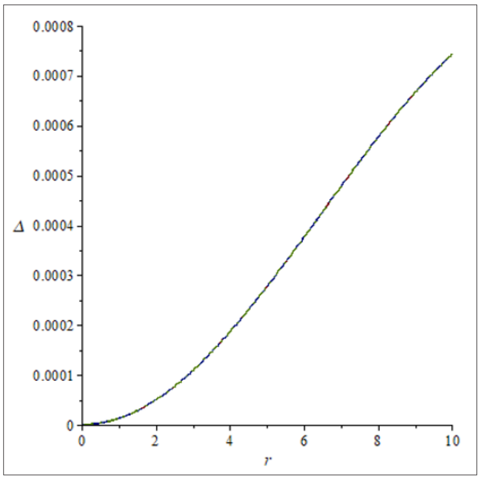

Figure 8: Anisotropy against the radial coordinate for A= 0.00003 (solid line), A= 0.00004 (long-dash line), A= 0.00005 (dash-dot line) and A=0.00006 (space-dot line). For all the cases a=0.001, α= 1/3 and β=0.000075

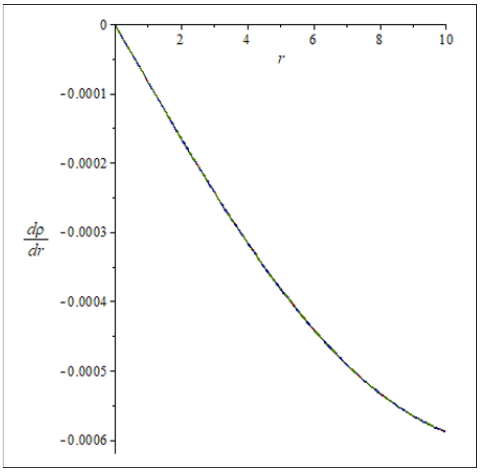

Figure 9: Energy density gradient against the radial coordinate for A= 0.00003 (solid line), **A**= 0.00004 (long-dash line), A= 0.00005 (dash-dot line) and A=0.00006 (space-dot line). For all the cases a=0.001, α= 1/3 and β=0.000075

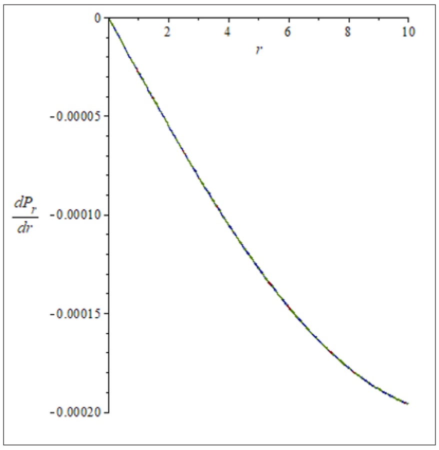

Figure 10: Radial pressure gradient against the radial coordinate for A= 0.00003 (solid line), A= 0.00004 (long-dash line), A= 0.00005 (dash-dot line) and A=0.00006 (space-dot line). For all the cases a=0.001, α= 1/3 and β=0.000075

Figure 1 shows the electric field intensity inside the star as a continually increasing function. As shown in Figure 2, for all values of A, the energy density is positive, continuous, and is a monotonically decreasing function throughout the stellar interior. The radial pressure is non-negative and falls as the radial parameter rises, as shown in Figure 3. Figure 4 display the behavior of the metric potential function $e^{2\nu}$ and shown that this function well behaved and presents a increment with the radial coordinate for all values of A, reaching the highest values when A=0.00006. In Figure 5 the gravitational potential $e^{2\lambda}$also is continuous and increases with the radial parameter. The mass function in Figure 6 is continuous, increasing, takes finite values, and behaves well in the interior of the star for all values of A taken into consideration. Figure 7 displays the surface red-shift profiles with the radial parameter and is it note that the surface redshift increases for all the values of A. In Figure 8 is it noted that the anisotropy Δ grows gradually for all selected A values and vanishes at the centre of the star. The radial variation of energy density gradient has been shown in Figure 9 and it is noted that $\frac{d\rho}{dr} < 0$ for all cases studied. Figure 10 shows that the profile of $\frac{dP_r}{dr}$ suggests that the radial pressure gradient inside the star is negative.

New solutions obtained in terms of elementary functions can be used to model compact objects with charge and anisotropy and these solutions can be related to some astronomical objects of interest. We can compare the estimated value for the mass with observational data of astrophysical object 4U1702-429 shown in Table 2 [40-41].

Table 2: Observed and calculated values of Stellar Masses and Surface Redshift for A=0.006and B=0.201257861

Stellar Object	Observed mass M(M$_\odot$)	Calculated mass M(M$_\odot$)	Surface redshift Z_S
4U1702-429	1.90	1.882599830	0.266451973

M$_\odot$= sun's mass

The behavior of the star's mass and surface redshift with the radial parameter for A= 0.0006 and B=0.201257861 is displayed in Table 3. The surface redshift is finite and nonsingular across the star where Z_S=0 at r=0, and the mass function increases as r increases.

The resulting mass is very similar to the low mass x-ray binary system 4U1702-429 [40-41]. The values found in this study using the linear equation of state for the mass, electric field and surface redshift for the binary system corresponding to 4U1702-429 are regular and behave well in the stellar interior.

Table 3: Variation of Mass M and Surface redshift Z_S for A= 0.0006 and B=0.201257861 from center to the surface of the star

r	M	Z_S
0	0	0
1	0.00199767937	0.002003685
2	0.01592724168	0.008060030
3	0.05346600750	0.018313046
4	0.12585481420	0.033031066
5	0.24384463900	0.052653656
6	0.41779762170	0.077867777
7	0.65793131450	0.109728494
8	0.97465833200	0.149854214
9	1.37894526900	0.200758210
10	1.88259983000	0.266451973

The dynamics of neutron star mergers, which produce the emission of gravitational waves suggesting the possible formation of heavy elements, and LIGO measurements of gravitational waves from a binary black hole merger [42] can both be predicted by simulations, especially when numerical relativity is applied. Advanced numerical relativity simulations have the ability to investigate phenomena like wormholes, peculiar stars, and quantum gravity effects in strong gravitational fields [43-44].

Conclusion

In this work, we solved Einstein-Maxwell field equations and built some simple relativistic charged star models with a static spherically symmetric locally anisotropic fluid distribution. By choosing a metric potential, figuring out the electric charge distribution, and applying the linear equation of state, we have investigated the fluid distribution behavior. An analytical stellar model with such physical properties could provide a good explanation of the internal structure of electrically charged odd stars. These newly found models are in full agreement with the Reissner-Nordström exterior metric exterior metric over the boundary r=R since matter variables and the gravitational potentials of this study are compatible with the physical analysis of these stars.

Physical properties such as matter, radial pressure, density, anisotropy, and charge density, as well as the plots generated, show that the proposed model performs well and may be compared to the binary system 4U1702-429. Predicting binary black hole mergers that produce gravitational waves and the dynamics of neutron star mergers that produce gravitational wave emission that suggests the formation of heavy elements, wormholes, exotic stars, and quantum gravity effects in strong gravitational fields are both possible with simulations, particularly when using numerical relativity.

The specific aim of our present approach is to demonstrate that by choosing appropriate constant parameters, we can rebuild models of various compact stars that are consistent with the available observational evidence. Therefore, the models considered in this research may have significant astrophysical relevance for scholars in this field.

References

1. Bicak J (2006) Einstein equations: exact solutions. Encyclopedia of Mathematical Physics 2: 165-173.
2. Kuhfitting PKF (2011) Some remarks on exact wormhole solutions. Adv Studies Theor Phys 5: 365-370.
3. Schwarzschild K (1916) On the gravitational field of a sphere of incompressible fluid according to Einstein's theory. Math Phys Tech: 424-434.
4. Chandrasekhar S (1931) The maximum mass of ideal white dwarfs. Astrophys J 74: 81-82.
5. Oppenheimer JR, Volkoff G (1939) On massive neutron cores. Phys Rev 55: 374-381.
6. Tolman RC (1939) Static solutions of Einstein's field equations for spheres of fluid. Phys Rev 55: 364-373.
7. Lobo FSN (2005) Stability of phantom wormholes. Phys Rev D 71: 124022.
8. Sushkov S (2005) Wormholes supported by a phantom energy. Phys Rev D 71: 043520.
9. Bibi R, Feroze T, Siddiqui A (2016) Solution of the Einstein-Maxwell equations with anisotropic negative pressure as a potential model of a dark energy star. Can J Phys 94: 758-762.
10. Chan R, da Silva MAF, Villas da Rocha JF (2009) On anisotropic dark energy. Mod Phys Lett A 24: 1137-1146.
11. Dayanandan B, Smitha TT (2021) Modelling of dark energy stars with Tolman IV gravitational potential. Chin J Phys 71: 683-692.
12. Lobo FSN (2006) Stable dark energy stars. Class Quant Grav 23: 1525-1541.
13. Malaver M (2013) Black holes, wormholes and dark energy stars in general relativity. Lambert Academic Publishing, Berlin.
14. Malaver M, Esculpi MA (2013) Theoretical model of stable dark energy stars. IJRRAS 14: 26-39.
15. Malaver M, Esculpi M, Govender M (2019) New models of dark energy stars with charge distributions. Int J Astrophys Space Sci 7: 27-32.
16. Malaver M, Kasmaei HD (2020) Analytical models of dark energy stars with quadratic equation of state. Appl Phys 3: 1-14.
17. Visser M (1995) Lorentzian wormholes: From Einstein to Hawking. AIP Press, New York, USA.
18. Sokolov AI (1980) Phase transitions in a superfluid neutron liquid. Sov Phys JETP 52: 575.
19. Usov VV (2004) Electric fields at the quark surface of strange stars in the color-flavor locked phase. Phys Rev D 70: 067301.
20. Bowers RL, Liang EPT (1974) Anisotropic spheres in general relativity. Astrophys J 188: 657.
21. Cosenza M, Herrera L, Esculpi M, Witten L (1981) Some models of anisotropic spheres in general relativity. J Math Phys 22: 118-125.
22. Thirukkanesh S, Ragel FC (2014) Strange star model with Tolman IV type potential. Astrophys Space Sci 352: 743-749.
23. Mak MK, Harko T (2004) Quark stars admitting a one-parameter group of conformal motions. Int J Mod Phys D 13: 149-156.
24. Malaver M, Iyer R (2024) Modelling of charged dark energy stars in a Tolman IV spacetime. Open J Astro 2: 000114.
25. Thirukkanesh S, Ragel FC (2012) Exact anisotropic sphere with polytropic equation of state. Pramana J Phys 78: 687-696.
26. Takisa PM, Maharaj SD (2013) Some charged polytropic models. Gen Relativ Gravit 45: 1951-1969.
27. Malaver M (2013) Analytical model for charged polytropic stars with Van der Waals modified equation of state. Am J Astron Astrophys 1: 41-46.
28. Malaver M (2013) Regular model for a quark star with Van der Waals modified equation of state. World Appl Program 3: 309-313.
29. Manjonjo AM, Maharaj SD, Moopanar S (2017) Conformal vectors and stellar models. Eur Phys J Plus 132: 62.
30. Rahaman F, Jamil M, Sharma R, Chakraborty K (2010) A class of solutions for anisotropic stars admitting conformal motion. Astrophys Space Sci 330: 249.
31. Jape JW, Sunzu JM, Maharaj SD, Mkenyeleye JM (2023) Charged conformal stars and equation of state. Indian J Phys 97: 1015.
32. Christopher J, Jape J, Sunzu JM (2024) Charged anisotropic conformal star model with a quadratic equation of state. Int J Mod Phys D 33: 2450022.
33. Kowa YK, Jape JW, Sunzu JM, Maharaj SD (2025) Anisotropic core-envelope compact star model with conformal symmetry. Indian J Phys. https: //doi.org/10.1007/s12648-025-03731-9.
34. Esculpi M, Alomá E (2010) Conformal anisotropic relativistic charged fluid spheres with a linear equation of state. Eur Phys J C 67: 521-532. https: //doi.org/10.1140/epjc/s10052-010-1273-y.
35. Malaver M, Esculpi M (2025) Some new models of charged dark energy stars in conformal symmetry. Rev Faraute Cienc Tecnol 16: 55-68.
36. Durgapal MC, Bannerji R (1983) New analytical stellar model in general relativity. Phys Rev D 27: 328-331.
37. Herrera L, Jimenez J, Leal L, Ponce de Leon J, Esculpi M, Galina V (1984) Anisotropic fluids and conformal motions in general relativity. J Math Phys 25: 3274.
38. Weyl H (1918) Reine infinitesimalgeometrie. Math Z 2: 384.
39. Delgaty MSR, Lake K (1998) Physical acceptability of isolated, static, spherically symmetric, perfect fluid solutions of Einstein's equations. Comput Phys Commun 115: 395.
40. Fan YZ, Han MZ, Jiang JL, Shao DS, Tang SP (2024) Maximum gravitational mass inferred at about 3% precision with multimessenger data of neutron stars. Phys Rev D 109: 043052.
41. Rocha L (2023) The masses of neutron stars. PhD Thesis. Univ São Paulo, Inst Astron Geofís Cienc Atmosf, Dept Astron, São Paulo, Brazil.
42. Swiggum JK (2023) The Green Bank North Celestial Cap Survey VII: 12 new pulsar timing solutions. Astrophys J 944: 154.
43. Bishop N, Rezzolla L (2016) Extraction of gravitational waves in numerical relativity. https: //arxiv.org/abs/1606.02532.
44. Gonzalez JA (2007) The inspiral and merger of binary black holes: numerical relativity and gravitational wave observatories. Phys Rev D 76: 124022.